Cell

Nuclear Architecture of Rod Photoreceptor Cells Adapts to Vision in Mammalian Evolution

Irina Solovei,[1] Moritz Kreysing,[2] Christian Lanctôt,[1,5] Süleyman Kösem,[1] Leo Peichl,[3] Thomas Cremer,[1,4] Jochen Guck,[2,*] and Boris Joffe[1,*]
[1]Division of Anthropology and Human Genetics, Biocenter, Ludwig-Maximilians University Munich, Grosshadernerstrasse 2, 82152 Planegg-Martinsried, Germany
[2]Department of Physics, Cavendish Laboratory, University of Cambridge, J.J. Thomson Avenue, Cambridge CB3 0HE, UK
[3]Max Planck Institute for Brain Research, Deutschordenstrasse 46, D-60528 Frankfurt am Main, Germany
[4]Munich Center for Integrated Protein Sciences (CiPS[M]), 81377 Munich, Germany
[5]Present address: Institute for Research in Immunology and Cancer (IRIC), Université de Montréal, P.O.Box 6128, Station Centre-ville, Montreal, Quebec H3C 3J7, Canada
*Correspondence: jg473@cam.ac.uk (J.G.), boris.joffe@lrz.uni-muenchen.de (B.J.)
DOI 10.1016/j.cell.2009.01.052

SUMMARY

We show that the nuclear architecture of rod photoreceptor cells differs fundamentally in nocturnal and diurnal mammals. The rods of diurnal retinas possess the conventional architecture found in nearly all eukaryotic cells, with most heterochromatin situated at the nuclear periphery and euchromatin residing toward the nuclear interior. The rods of nocturnal retinas have a unique inverted pattern, where heterochromatin localizes in the nuclear center, whereas euchromatin, as well as nascent transcripts and splicing machinery, line the nuclear border. The inverted pattern forms by remodeling of the conventional one during terminal differentiation of rods. The inverted rod nuclei act as collecting lenses, and computer simulations indicate that columns of such nuclei channel light efficiently toward the light-sensing rod outer segments. Comparison of the two patterns suggests that the conventional architecture prevails in eukaryotic nuclei because it results in more flexible chromosome arrangements, facilitating positional regulation of nuclear functions.

INTRODUCTION

In interphase nuclei, heterochromatin and euchromatin form distinct, spatially separated domains (Kosak et al., 2007; Misteli, 2007). Heterochromatin is more condensed and typically enriched at the nuclear envelope and around the nucleoli, while the less condensed euchromatin is distributed in the nuclear interior between the perinuclear and perinucleolar heterochromatin compartments. Although cell type-specific variants of nuclear architecture can differ notably in details, the pattern described above is nearly universal. Below we refer to this architecture as the conventional one. It is conserved in evolution from unicellular to multicellular organisms (Postberg et al., 2005) and is also reflected by the spatiotemporal pattern of DNA replication (Ferreira et al., 1997; Sadoni et al., 1999). Major deviations from the conventional architecture are known only in some unicellular organisms: Dinoflagellata, some yeast species, and macronuclei—but not the cycling micronuclei—of ciliates (Postberg et al., 2005).

The reason for the evolutionary stability of nuclear architecture is most probably the important role that the spatial arrangement of chromatin plays in transcriptional regulation (Fraser and Bickmore, 2007; Sexton et al., 2007). The nuclear lamina and the border of the nucleoli form the major repressive nuclear compartments (Guelen et al., 2008; Zhang et al., 2007). Some genes are repositioned from the nuclear periphery to the interior, when they become active (Chuang et al., 2006; Dundr et al., 2007; Lanctot et al., 2007). The active alleles of genes with monoallelic expression take more internal nuclear positions than their inactive counterparts (Takizawa et al., 2008). Targeting to the nuclear periphery suppresses transcription of some, but not all, genes (Finlan et al., 2008; Kumaran and Spector, 2008; Reddy et al., 2008). Recent studies have also demonstrated that the surrounding of the nuclear pores actually may form a domain of intense transcription at the nuclear periphery (Akhtar and Gasser, 2007). Nevertheless, most of the transcribed genes are located in the nuclear interior (Kosak et al., 2007).

In view of the pivotal role that nuclear architecture plays in the regulation of nuclear functions, it is of great interest that the nuclei of mouse rod photoreceptors show a very different pattern, where the central portion of the nucleus is occupied by a large mass of heterochromatin, while transcription factors are enriched at the nuclear periphery (Carter-Dawson and LaVail, 1979; Helmlinger et al., 2006). We call this nuclear architecture inverted. Here, we present a detailed analysis of the inverted pattern, demonstrate that it is an adaptation to nocturnal vision (specific to mammals), and discuss implications of our findings for the understanding of the conventional nuclear architecture.

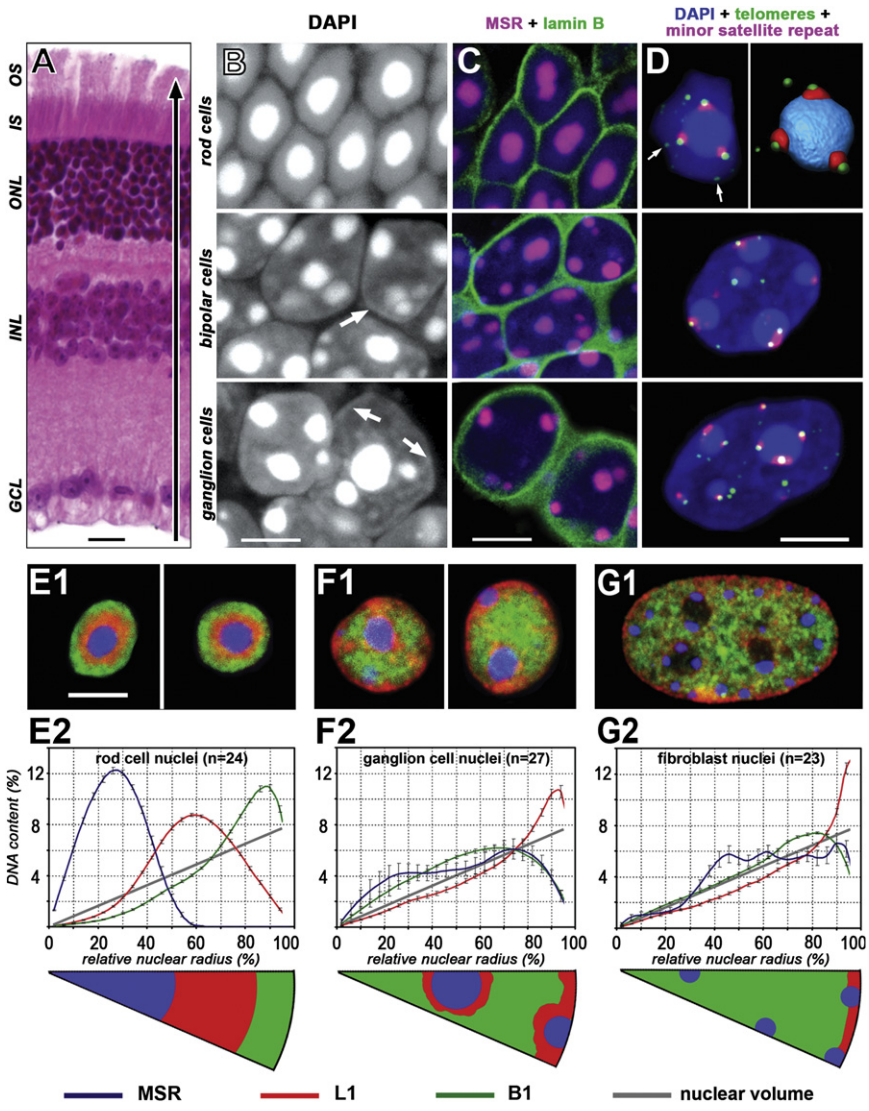

Figure 1. Nuclear Architecture of Mouse Rods in Comparison to Other Cells

(A) Organization of the mouse retina (arrow shows the direction of light): ganglion cell layer (GCL), inner nuclear layer (INL; mainly perikarya of bipolar cells), outer nuclear layer (ONL; perikarya of the photoreceptor cells), and inner (IS; cytoplasmic) and outer (OS; light-sensing) segments of the photoreceptor cells; hemalaun-eosin staining.

(B–D) Organization of rod, bipolar, and ganglion cells.

(B) DAPI counterstain. Note the difference in the chromocenter number and a rim of heterochromatin along the nuclear border (arrows) lacking in rods.

(C) Major satellite repeat (MSR; marker of chromocenters, red); nuclear lamina labeled with anti-lamin-B (green).

(D) Centromere clusters (minor satellite repeat probe, red), telomere DNA (green), and chromocenters (counterstain, blue). The top right image shows a 3D reconstruction of a rod chromocenter (note a distal telomere cluster at some distance from the chromocenter).

(E–G) Radial distribution of constitutive heterochromatin (MSR, blue), L1-rich heterochromatin (L1, red), and euchromatin (B1, green) in the nuclei of rods (E), ganglion cells (F) and fibroblasts (G).

(E1–G1) Mid optical sections of nuclei.

(E2–G2) Radial distribution graphs (n = 20–25). Error bars are approximate 95% confidence intervals; straight lines show the distribution of the nuclear volume. Sectors in the bottom row schematically show the chromatin distribution.

Scale bars represent 20 μm (A) and 5 μm (B–G).

RESULTS

The mouse retina consists of several distinct layers formed by neuronal perikarya or their processes (Figure 1A). The retina of all vertebrates is inverted: to reach the sensory portions of the photoreceptors (the outer segments), light has to pass through the entire thickness of the retina. The outer segments are joined to the inner segments, the portions of photoreceptor cells where most cytoplasmic processes occur. The perikarya of photoreceptor cells have only a very thin layer of cytoplasm and are found in the outer nuclear layer (ONL). In the mouse, a specialized nocturnal animal, 97% of the photoreceptor cells are highly sensitive rod cells that serve nocturnal black-and-white vision. Cones, which mediate color vision, comprise only 3% of photoreceptors. Perikarya of retinal interneurons are located in the inner nuclear layer (bipolar, horizontal, and amacrine cells) and ganglion cell layer.

Mouse rod cells look strikingly unusual even after simple staining with DAPI. In all mouse cells, including other retinal cells, it brightly stains several (usually six to seven) chromocenters adjoining the nuclear periphery or the nucleolus (Figure 1B), and a rim of condensed chromatin along the nuclear border (arrows). In contrast, rods have a single very large central chromocenter and no staining at the nuclear border. To understand the spatial organization of these unusual nuclei, we studied the distribution of euchromatin and heterochromatin using fluorescence in situ hybridization (FISH) for marker repetitive sequences.

Chromatin of Mouse Rod Nuclei Is Arranged in a Concentric Fashion According to Gene Density

Centromeres and telomeres were detected by FISH with the minor satellite repeat probe and pantelomere probe, respectively. In rod nuclei, clusters of centromeres (three to five per nucleus) were found only on the surface of the chromocenters; each centromere cluster was associated with a cluster of telomeres (Figure 1D). Since all mouse chromosomes are acrocentric, these clusters were obviously formed by the proximal telomeres that are directly adjacent to the centromeres. Distal telomeres were predominantly distributed in the layer of peripheral chromatin (Figure 1D, arrows). Other retinal cells had more (6–18) clusters of centromeres, and their distal

telomeres were usually located in the inner nuclear regions (Figure 1D).

Next, we determined the spatial distribution of the repetitive sequences characteristic of the C, G, and R bands of mouse chromosomes, which correspond to subcentromeric satellite DNA (constitutive heterochromatin, present on all mouse chromosomes and localized to the chromocenters), gene-poor mid-late replicating noncentromeric heterochromatin (L1-rich heterochromatin), and gene-dense early-replicating chromatin (euchromatin), respectively. To this end, we used probes for MSR (C bands), L1 (the major class of the long interspersed repetitive sequences; G bands) and B1 (the major class of the short interspersed repetitive sequences related to human *Alu* sequences; R bands) (c.f. Waterston et al., 2002). The chromosomal distribution of the used probes was confirmed by FISH on metaphase spreads (Figure S1 available online). In rod nuclei, FISH on cryosections revealed a single MSR-positive chromocenter surrounded by a thick shell of L1-rich chromatin and a thin outer shell of B1-rich euchromatin (Figures 1C1 and 1E1). By contrast, ganglion cells (Figure 1F1), bipolar cells, and cones (Figures S2A and S2B) showed the conventional nuclear architecture: B1-rich gene-dense chromatin was found toward the interior of the nucleus, whereas L1-rich gene-poor chromatin adjoined the nuclear border and surrounded the chromocenters. This pattern was also found in cultured mouse embryonic fibroblasts, with the exception that we did not observe L1-rich chromatin around the chromocenters (Figure 1G1). Quantitative evaluation of the radial distribution (Figures 1E2–1G2) confirmed the dramatic difference in the spatial distributions of marker DNA sequences between rods and cells with the conventional nuclear architecture.

Genes Are Positioned at the Periphery of Mouse Rod Nuclei Irrespective of Their Transcriptional Status

To obtain more detailed information about the unusual peripheral localization of gene-rich chromatin, we analyzed the nuclear localizations of three groups of genes: (1) ubiquitously expressed housekeeping genes, (2) genes expressed specifically in rod cells, and (3) genes specifically expressed in nonretinal cells and silent in the retina (Blackshaw et al., 2001) (Ensembl Database; see Figure S3 for chromosomal locations of these genes). The ubiquitously expressed genes were β-actin (*Actb*), α-tubulin (*Tuba1*), and nucleophosmin (*Npm1*); genes expressed specifically in rod cells were phosducin (*Pdc*), retinitis pigmentosa 1 homolog (*Rp1h*), rod outer segment membrane protein 1 (*Rom1*), and rod opsin (*Rho*); and genes silent in the retina were lysozyme (*Lyzs*), hemoglobin alpha adult chain 1 (*Hba-a1*), and hair keratin (*Krt1-1*). DNA probes for genes of each group were pooled (pools 1, 2, and 3, respectively), labeled, and hybridized pairwise (pools 1+2 and pools 2+3) to vibratome sections of mouse retina, thus allowing us to compare the positioning of transcriptionally active and inactive genes in the same cells.

In rod cells, all genes, irrespective of their transcriptional status, were localized toward the nuclear periphery, in most cases juxtaposed to the nuclear lamina (Figures 2A–2C). This peripheral localization is particularly obvious upon visualization of the nuclear lamina with antibodies to lamin in the regions where nuclei were cut tangentially (Figures 2A and 2A′, arrows). In particular, genes located next to the subcentromeric heterochromatin also had peripheral positions in rod nuclei (Figure S4). In ganglion and bipolar cells, genes were found throughout the nuclear space (Figures 2D–2F). We also estimated the preferred location of the studied genes as described by Ronneberger et al. (2008). In rods, all genes were preferentially localized within 600 nm of the nuclear border (Figure 2G); an ~1.5-fold excess of genes observed in this layer was statistically significant ($p = 0.01$). In ganglion cells, genes were underrepresented in this outer layer and shifted toward the nuclear center (Figure 2H).

An earlier study had shown that the periphery of rod nuclei is enriched in transcriptional factors (Helmlinger et al., 2006). We performed RNA FISH with an oligonucleotide probe for transcripts of the rod opsin gene, the most highly transcribed gene in rods (Blackshaw et al., 2001). Nascent transcripts were found exclusively at the periphery of rod nuclei (Figures 2I–2N). The position of the nucleoli—where rDNA is intensely transcribed—was determined with antibodies against pB23. In agreement with the results obtained with rod opsin gene, the nucleoli of rod cells had a peripheral position at the border between the euchromatic and heterochromatic shells, in a noteworthy difference to the typically internal location of the nucleoli in other cells. Finally, immunostaining of nuclear speckles (anti-SC35) and U2 snRNPs (anti-SF3b66) showed that splicing machinery was also localized to the narrow peripheral shell of the rod nuclei (Figures 2O–2R).

The Distribution of Histone Modifications Confirms the Inverted Architecture of Mouse Rod Nuclei

Several histone modifications have been shown to accumulate specifically on transcriptionally active and repressed chromatin (reviewed in Martens et al., 2005). In mouse rod cells, euchromatin marker H3K4me3 was detected exclusively at the nuclear periphery, while in ganglion and bipolar cells, as well as in cultured mouse embryonic fibroblasts, it was observed throughout the nuclear interior (Figures 3A and S5). Heterochromatin markers H3K9me3 and H4K20me3 were restricted to chromocenters in mouse fibroblasts (Figure S5). In bipolar and ganglion cells, H4K20me3 was found in chromocenters and in the heterochromatin rim along the nuclear border and around chromocenters (Figure 3B, thick arrows). In rods, H3K9me3 signals were restricted to the chromocenters (Figure 3C), whereas anti-H4K20me3 marked the shell of L1-rich heterochromatin around them. To reveal this histone modification inside the chromocenters (Figure 3B), an extended antigen retrieval was necessary (30 min instead of 5 min used in other cases). The distribution of histone modifications in cone nuclei was consistent with the conventional pattern (Figures S2C–S2E). In summary, the data on histone modifications in rod nuclei corroborated the concentric inverted distribution demonstrated by FISH with marker DNA sequences (c.f. Figures 3D and 1E–1G).

The Inverted Pattern Is Established during Terminal Differentiation of Rod Nuclei

In mouse, proliferation of rod progenitors in the central retina ceases 5 days after birth (P5), the eyes open at P13, and sexual

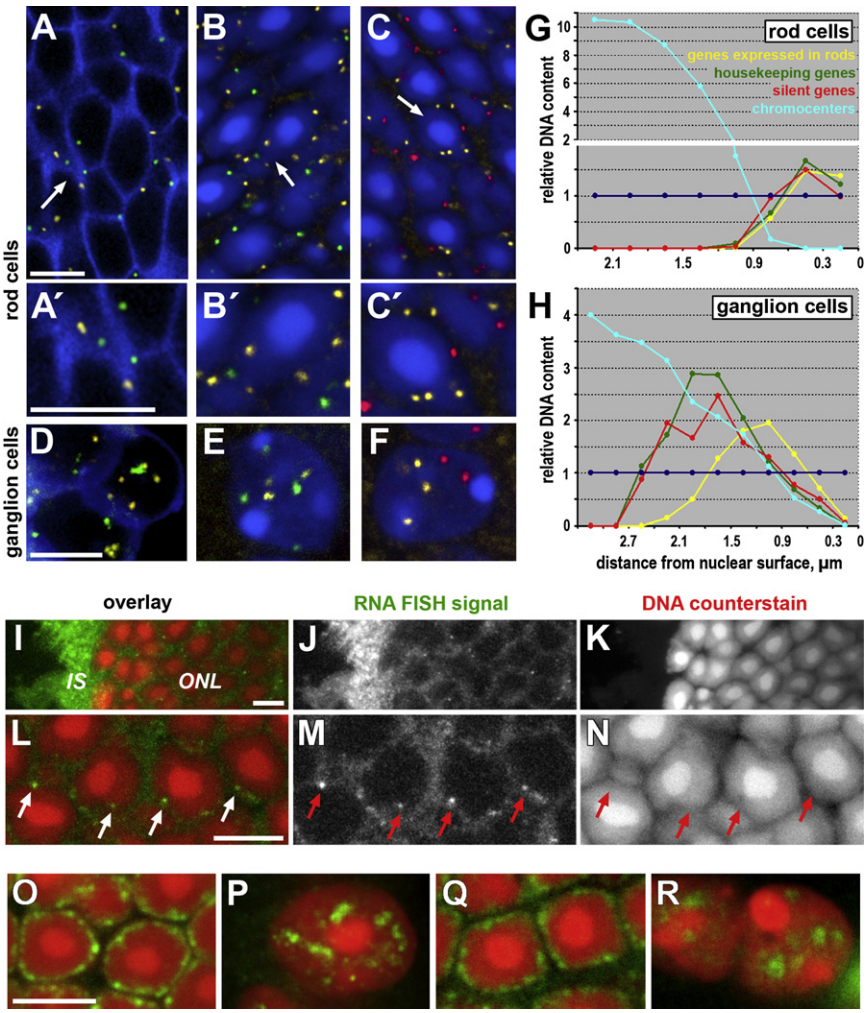

Figure 2. Spatial Distribution of Genes and Localization of Nascent Transcripts and Splicing Machinery in Mouse Rod and Ganglion Cell Nuclei

(A–H) Positioning of genes specifically active in rods (yellow), housekeeping (green), and silent in rods (red) in the nuclei of rods (A–C) and ganglion cells (D–F). The nuclear border was stained with antibodies against lamin B ([A] and [D], blue) or all nuclear DNA was stained with DAPI ([B], [C], [E], and [F], blue). Peripheral positions of all genes in rods are especially clear in the regions where nuclei were cut tangentially (arrows in [A]–[C], enlarged in [A′]–[C′]). Graphs (G–H) quantify the radial distribution of the analyzed genes (n = 24–28). The dark blue horizontal line corresponds to the uniform (no preference) distribution of signals.

(I–N) Peripheral localization of the nascent transcripts of rod opsin gene (green; nuclear counterstain, red). Strong cytoplasmic RNA signal is observed in the inner segments of rods (*IS*) where transcripts accumulate for protein synthesis (I and J), while cytoplasmic RNA signal around the rod nuclei (*ONL*) is relatively weak (J and M). Foci of nascent RNA transcripts ([L] and [M], arrows) are seen only at the nuclear periphery.

(O–R) Nuclear speckles ([O] and [P], green) and U2 snRNP ([Q] and [R], green) in rod nuclei (O and Q) and nuclei of ganglion cells (P and R).

Scale bars represent 5 μm.

maturity is reached at P28. We studied mouse retinas dissected at birth (P0), P6, P14, P21, P28, and 9 months (Figure 4). We performed FISH with markers for constitutive heterochromatin (MSR), L1-rich heterochromatin (L1), and euchromatin (B1) (Figures 4A and 4C). At P0, rod nuclei had a conventional architecture: the L1 signal was found at the nuclear periphery and around the chromocenters, whereas the B1 signal occupied a more internal position. At P6, L1-rich chromatin started to accumulate around the chromocenters and to disappear from the nuclear periphery. At P14 and P21, L1-rich chromatin was found exclusively around the chromocenters. By P28, the conventional arrangement was completely transformed into the inverted one. In the course of this remodeling, the median number of chromocenters decreased from about 13 at P0 to two at P28 (45% of nuclei had one chromocenter, 5% had three chromocenters). At 9 months, all rods showed a single chromocenter (Figures 4A and 4B). Concomitantly, the median diameter of chromocenters increased from 1.2 μm to 2.8 μm ($p < 0.001$, Mann-Whitney test), suggesting that chromocenters fused during terminal differentiation. Indeed, we observed a number of sandglass-shaped chromocenters suggestive of ongoing fusions (Figure 4D).

Labeling of marker histone modifications at various stages of rod cell differentiation confirmed the data obtained with marker chromatin sequences. The H3K4me3 signal, which occupied the center of rod nuclei at P0, gradually relocated to a thin shell along the nuclear border (Figure 4E). Nucleoli also moved toward the nuclear periphery (Figures 4E and 4F). At P0, chromocenters could be stained with anti-H4K20me3 after 5 min of antigen retrieval, while starting from P14 visualization of H4K20me3 in chromocenters required prolonged antigen retrieval (c.f. Figures 4F and 3B). Rod cell differentiation was also accompanied by a change in the nuclear shape from ellipsoidal to spherical (Figures 4A and 4H) and a decrease in nuclear volume by about 40% (Figure 4G). Though remodeling doubtlessly demands complicated relocations of chromatin, the final difference in the distribution of eu- and heterochromatin seems to primarily depend on a difference in the location and orientation of chromosome territories (Figures 4I–4K; see Discussion for more details).

The Inverted Nuclear Architecture Correlates with Nocturnal Lifestyle

In addition to mouse, we examined the distribution of marker histone modifications in 16 species from distant groups of terrestrial mammals (Figures 5A–5E and S6). Within several groups we found species with the inverted pattern and species with the conventional one. Only moderate modifications of the inverted

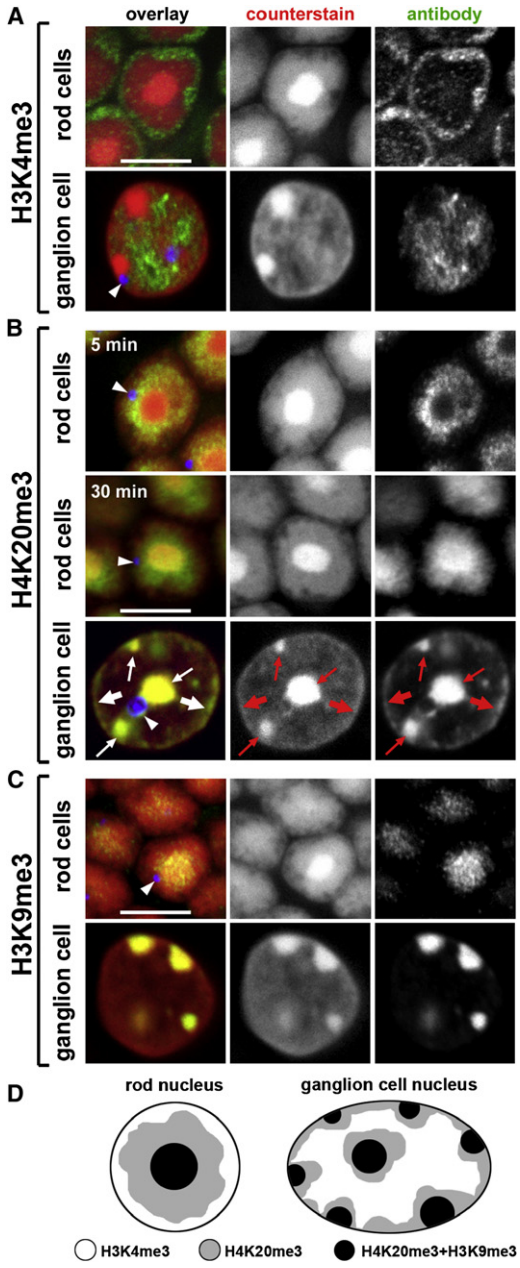

Figure 3. Distribution of Marker Histone Modifications in Mouse Rod and Ganglion Cell Nuclei

Antibody staining for histone modifications (green), nucleolus (blue, arrowheads), and nuclear counterstain (red).

(A) H3K4me3 (euchromatin).

(B) H4K20me3 (heterochromatin); staining after the usual (5 min, rod chromocenters remain unstained) and prolonged (30 min) antigen retrieval. In ganglion cells, chromocenters (thin arrows) get stained after 5 min antigen retrieval; in these cells, anti-H4K20me3 also marks small amounts of heterochromatin around the chromocenters and a narrow shell along the nuclear border (wide arrows).

(C) H3K9me3 (constitutive heterochromatin).

(D) Schemes summarizing the distribution of marker histone modifications in rod nuclei and in ganglion cells representing the conventional pattern.

Scale bars represent 5 μm.

pattern were observed between species (Figure 5C). The nuclei were either nearly spherical (as in the mouse) or elongated, in which case they had a single central heterochromatin mass with a shape suggestive of an incomplete fusion of two (or even three) heterochromatin clusters located along the long axis of the nucleus (c.f. Figures 4 and S6). In such nuclei, H3K4me3-positive transcriptionally active chromatin was present not only along the nuclear periphery but also in concavities of the heterochromatin mass (Figure S6A). As in the mouse, the nucleoli (several per cell) were always small and localized to the border between eu- and heterochromatin (Figures 5A and S6). By contrast, rod nuclei with the conventional pattern always showed a clear rim of heterochromatin along the nuclear envelope (Figures 5B and S6, arrows), whereas transcriptionally active chromatin and nucleoli (of usual size) were located in the inner nuclear regions. In some species (e.g., pig and chipmunk), internal clusters of heterochromatin were observed in a proportion of nuclei in association with the nucleoli. Only rod nuclei of the cow had an intermediate pattern (Figures 5D and S6); in some sectors, the nuclear border was lined by euchromatin, while in other sectors heterochromatin reached the nuclear periphery. Rare "tongues" of heterochromatin running to the nuclear periphery were also observed in several other species, but they interrupted the euchromatin shell lining the nuclear border to only a very small degree.

Our data revealed a wholly unexpected but very clear correlation between the rod nuclear architecture and lifestyle (Figure 6) that was further supported by data on 22 additional species (Tables S1 and S2). Nocturnal mammals had the inverted pattern, while the diurnal ones showed the conventional one. Crepuscular species (active predominantly at dusk and dawn) had either the inverted pattern (e.g., crepuscular to nocturnal deer species) or the conventional one (e.g., zebra and horse that form larger herds and are more active during the day). Even clearer than it did with lifestyle, nuclear architecture correlated with the key features of retinal adaptation to scotopic (low-light) or photopic (daylight) vision (Ahnelt and Kolb, 2000; Peichl, 2005), namely the areal density of rods, the number of tiers of perikarya in the outer nuclear layer, and the percentage of cones (Figure 6B). Only in guinea pig was an inverted pattern found in a "diurnal" retina, which probably reflects ongoing adaptation to a diurnal lifestyle (see comments accompanying Figure S15). Nuclei with the inverted pattern also have a smaller size than nuclei with the conventional pattern (Figure 5F). This correlation did not depend on genome size (Figure S7), which is rather constant in mammals (Gregory et al., 2007).

Inversion of Rod Nuclear Architecture Alters Light Transmission through the ONL

The correlation between the inverted nuclear architecture and night vision suggested that the inverted pattern might have an optical ramification. Nocturnal mammals see at light intensities a million times lower than those available during the day, and their rod photoreceptors possess a light sensitivity down to the level of a few photons (Sterling, 2003). This high sensitivity rests primarily on the high density and small size of the outer segments (OS, Figure 1A) and therefore demands a large number of rod cells, which increases the thickness of the ONL (Sterling, 2003;

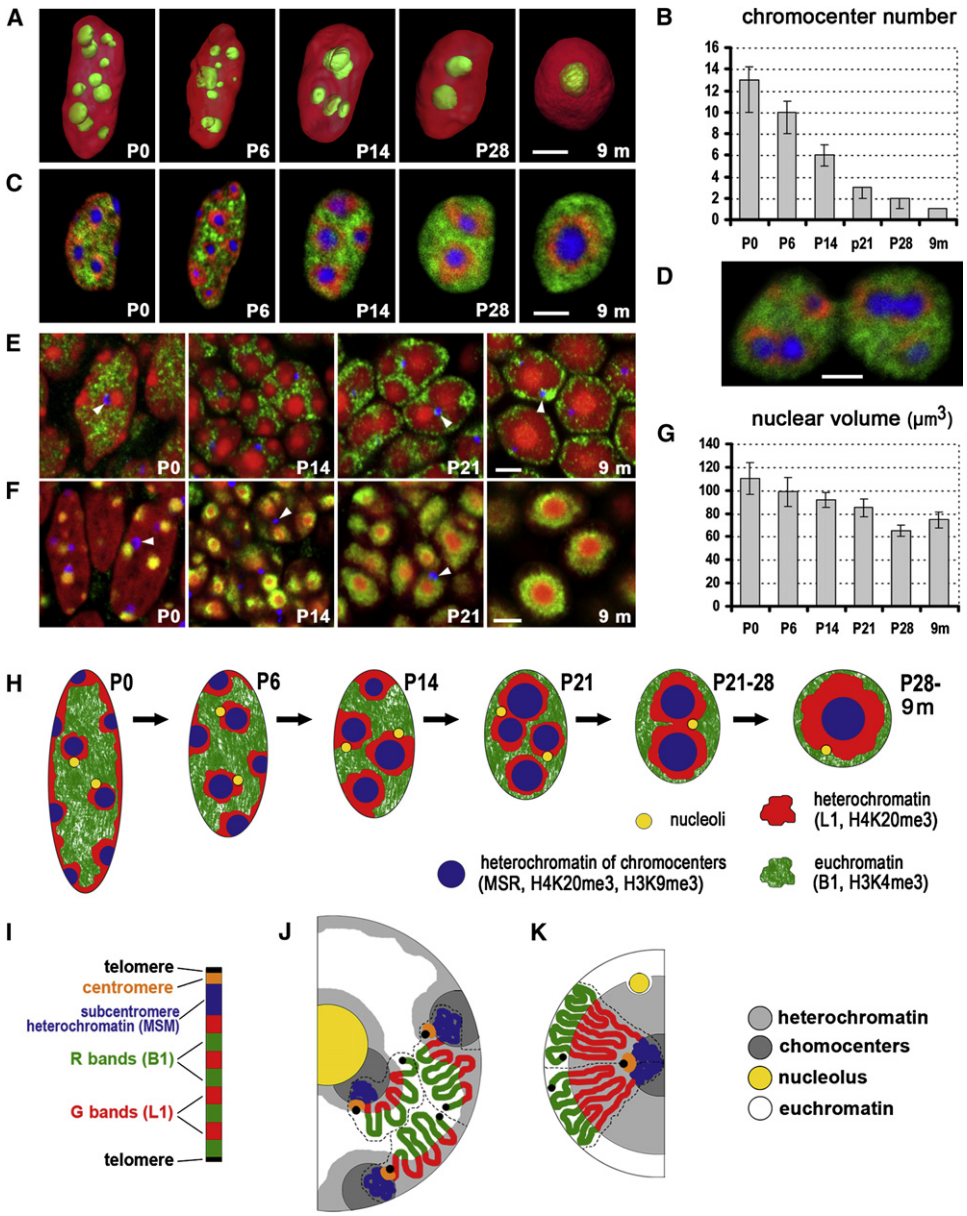

Figure 4. Inversion of the Nuclear Architecture during Terminal Differentiation of Mouse Rods

The organization of the rod nuclei in postnatal development (P0–P28) and in a 9-month-old mouse (9 m).

(A and B) Changes in the number of chromocenters and the shape of the nucleus. The graph (B) shows the median chromocenter number per nucleus. Error bars show 95% confidence intervals.

(C and D) FISH with probes for L1 (L1-rich heterochromatin, red), B1 (euchromatin, green), and MSR (chromocenters, blue). Putative fusions of chromocenters were observed (D). Neighboring nuclei were erased in (C) and (D).

(E and F) The distribution of marker histone modifications H3K4me3 ([E], euchromatin) and H4K20me3 ([F], heterochromatin): antibody staining after 5 min antigen retrieval; histone modifications (green), nucleoli (blue, arrowheads), and nuclear counterstain (red).

(G) Changes of estimated mean nuclear volume. Error bars show 95% confidence intervals.

(H) Scheme of the remodeling of the nuclear architecture.

(I–K) Scheme of the distribution of chromosome subregions (I) in interphase nuclei with the conventional (J) and inverted (K) architecture.

Scale bars for (A)–(F) represent 2 μm.

Williams and Moody, 2003). The optimization of light transmission through the ONL could therefore provide crucial advantages for nocturnal vision.

Live-cell observations of retinal cells in freshly isolated retina from an adult mouse by brightfield microscopy showed that inverted rod nuclei were transparent and little distorting for

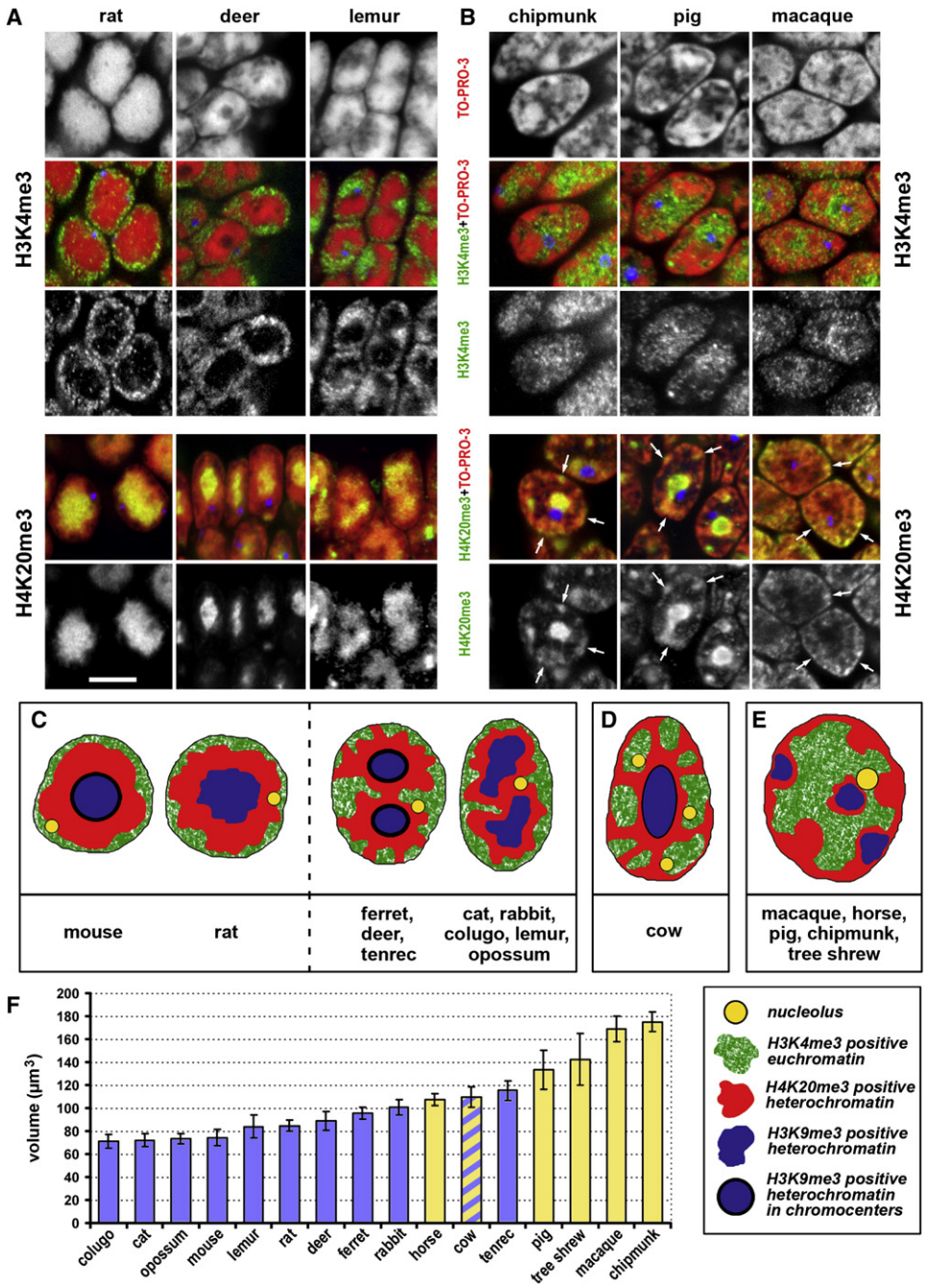

Figure 5. Rod Nuclear Architecture of Different Mammalian Species

(A and B) Inverted (A) and conventional (B) rod nuclear architecture in representatives of Rodentia (rat, chipmunk), Artiodactyla (deer, pig), and Primates (lemur, macaque): the distribution of marker histone modifications (green), nucleoli (blue), and nuclear counterstain (red). The scale bar represents 5 μm. The distributions of H3K4me3 and H4K20me3 for further species are shown in Figure S6.

(C–E) Schematic representation of the inverted (C), intermediate (D), and conventional (E) nuclear architecture in 16 species (c.f. Figure 6); for color code, see the bottom-right panel.

(F) Rod nuclei with the inverted pattern (blue columns) have smaller mean volume than those with the conventional pattern (yellow columns). Error bars show 95% confidence intervals.

visible light (Figure 7A1). Using phase contrast, we observed a central dark area occupying most of the rod nucleus surrounded by a lighter rim (Figure 7A2). This observation indicates a higher refractive index of the central dark area and a lower refractive index of the nuclear rim, in remarkable correspondence to the distribution of hetero- and euchromatin after

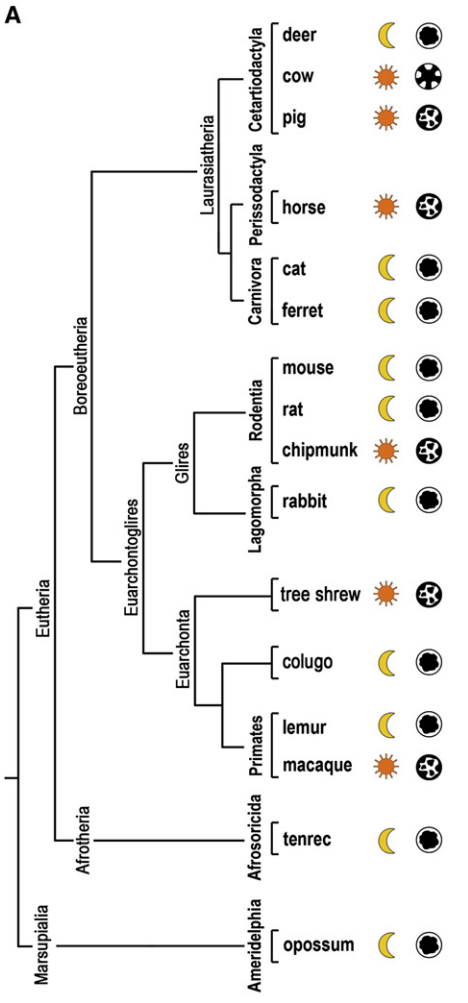

B

species	peak rod density, $10^3/mm^2$	number of ONL tiers	peak percent of cones	activity
mouse lemur	850	14	1%	N
opossum	530	10	1%	N
mouse	500	11	3%	N
cat	460	12	9%	N + C
fallow deer	460	10	8%	C+N,D
rat	400	12	1%	N
ferret	350	9	8%	N
rabbit	300	6	6%	N + C
cow	270	8	9%	D + C
tenrec	255	8	2%	N
macaque	184	7	100% (fovea)*	D
colugo	170	8	7%	N
horse	170	4	10%	C+D,N
pig	115	7	16%	D
chipmunk	6.5	3	80%	D
three shrew	3.5	1	86%	D

* average: 5%

nocturnal / crepuscular activity (N, C)
diurnal activity (D)

inverted pattern
conventional pattern
intermediate pattern

Figure 6. Nuclear Architecture of Mammalian Rods Correlates with Lifestyle and the Organization of the Retina

(A) Both the inverted and conventional architecture of rod nuclei is represented in various evolutionary branches of mammals and correlate with the lifestyle (tree topology based on Murphy et al. [2001]).

(B) Correlation of the nuclear pattern (inverted, gray; conventional, yellow; intermediate, striped) with the key parameters characterizing adaptation of the retina to nocturnal or diurnal vision. The table presents maximal values found in the literature or measured by us (for details, see the Supplemental Experimental Procedures).

staining performed by us and in transmission electron microscopy (TEM) images of mouse rods (Figure S8). By contrast, nuclei with the conventional pattern were optically heterogeneous on length scales comparable to the wavelength of light (Figure 7A3) and showed a complex pattern of regions with varying refractivity associated with heterochromatin structures such as chromocenters and the peripheral heterochromatin rim (Figure 7A4), which causes more scattering.

To illuminate the effect of this difference in refractive index on the light transmission through rod cell perikarya, we performed computer simulations using a finite-difference time-domain (FDTD) algorithm (Farjadpour et al., 2006). For simulation of the inverted nuclei, we used the size parameters of the mouse rods: the diameter of 5 μm and the ratio of the outer euchromatin shell width to the radius of the heterochromatic core of 1:4 (the volume ratio of heterochromatin and euchromatin is about unity). Conventional nuclei were modeled with the regions interchanged. We used refractive indices of 1.385 and 1.415 for the euchromatin and heterochromatin regions, respectively, and 1.360 for the surrounding tissue. The wavelength of light chosen for the simulation was 500 nm, to match the peak sensitivity of the rod photoreceptors (see the Supplemental Experimental Procedures for justification of the used parameter values). Our computer simulations showed that nuclei with inverted pattern are converging lenses, while those with the conventional one are little more than diffractive obstacles (Figure 7B). This finding was robust against variations in relative and absolute shell/core size, specific values for the refractive indices, and wavelength (Figure S9).

To experimentally verify the simulated focusing behavior of rod nuclei, we studied isolated rod cells with the inverted and the conventional nuclear architecture using a Jamin-Lebedev interferometric phase microscope that allows the direct quantitative measurement of phase retardation (phase shift) of light passing through objects with diffraction-limited resolution. The phase shift distribution depends on both refractive index and thickness, fully describes the properties of this object as an optical element, and allows reconstruction of its focusing behavior (Figure S10). The results of phase shift measurements corresponded fully to the observed distributions of heterochromatin (Figure 7A) and our simulation of the inverted and conventional nuclei (Figure 7B). Profiles for inverted mouse rod nuclei had a parabolic shape characteristic of a focusing (convex) lens, whereas profiles for the conventional pig rod nuclei were clearly different, top hat shaped (Figures 7C1–7C3 and S11). Fusion of chromocenters in the rods of young mice results in local maximums in the phase shift profiles. Evaluation of the phase retardation profiles (Figure 7C4) confirmed a much stronger focusing and less scattering of light by the inverted nuclei compared to nuclei with the conventional architecture predicted by our simulations for model nuclei with idealized shape.

The lensing capability of single inverted rod nuclei needs to be considered in the context of the ONL where rod nuclei are arranged in columns (Figures 7D1 and 7D2). These columns are well documented and predetermined by embryogenesis of the retina (Reese et al., 1995; Acosta et al., 2008). Therefore,

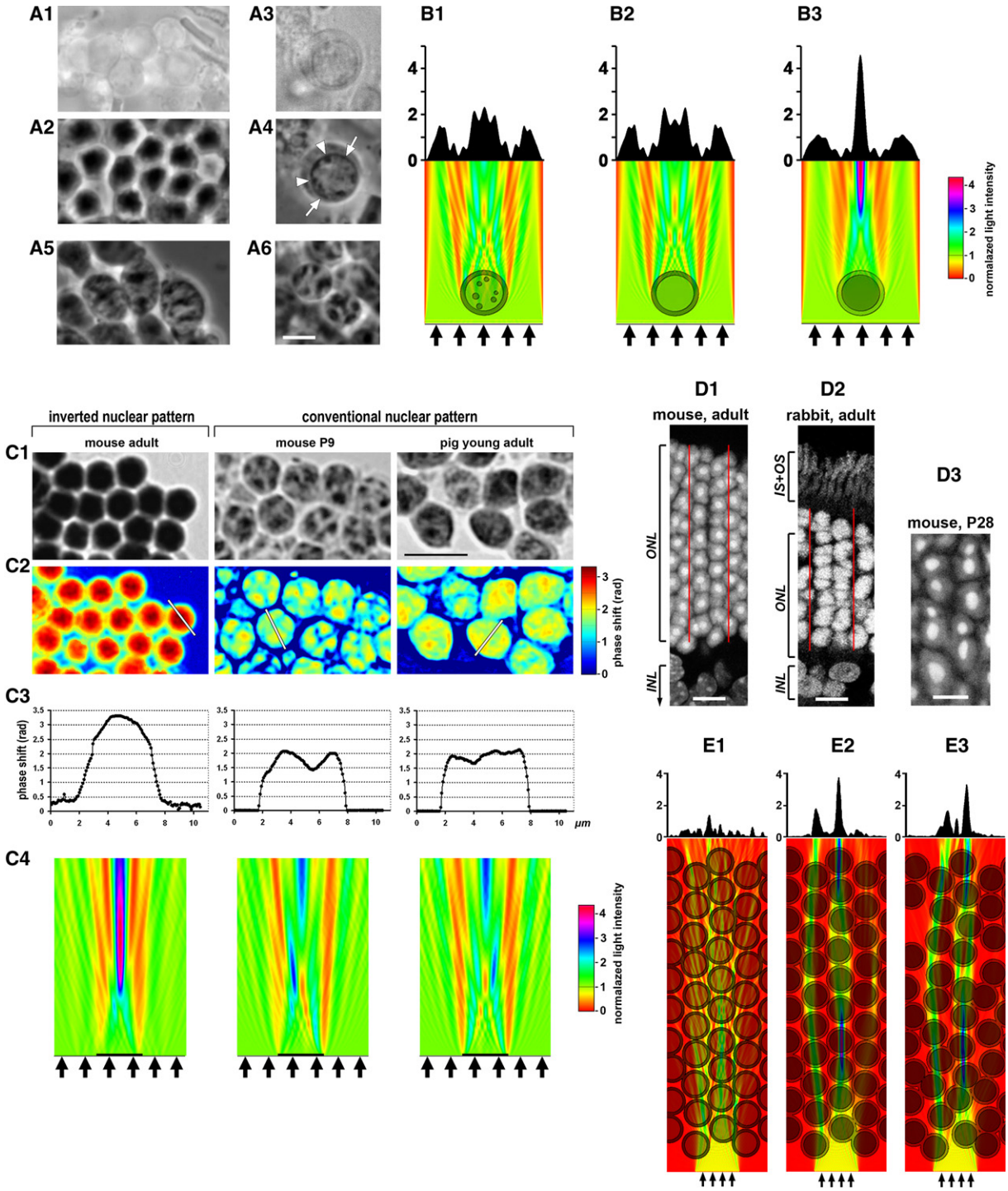

Figure 7. Optical Properties of Rod Nuclei in Mammalian Retina

(A) Nuclei of living retinal cells with the inverted (A1 and A2) and conventional (A3–A6) pattern in bright field (A1 and A3) and with phase contrast (A2 and A4–A6). Mouse rods (the same cells; A1 and A2), a cell from the INL layer (A3 and A4), pig rods (A5), and rods of young (P12) mouse (A6) are shown. Note that heterochromatin appears dark in phase contrast images, indicating a higher refractive index. The scale bar represents 5 μm.

(B) FDTD simulations of light propagation (in the direction shown by arrows) through single nuclei with a conventional pattern (B1), with a peripheral rim of higher refractive material (B2), and with inverted pattern (B3). The light intensities (normalized to the incident intensity) are shown by intensity profiles for the top margin of images and color-coded for the other parts of images.

(C) Phase retardation measurements of light passing through rod nuclei with inverted and conventional architecture. C1 shows raw phase images taken on a compensated Jamin-Lebedev interferometric microscope. The scale bar represents 10 μm. C2 shows false-color maps of phase retardation. The color

we simulated propagation of a spatially confined plane wave through the ONL with hexagonally packed perikarya. The centers of the nuclei were randomly displaced by a small amount to better resemble the situation in vivo where columns are not ideally regular. The other parameters used for this simulation were the same as for the single nuclei. In contrast to the conventional nuclei where light was scattered strongly and spread out into adjacent columns (Figure 7E1), in columns of inverted nuclei scatter was low: right after the ONL (i.e., at the level of photoreceptor input), light from different columns practically did not mix (Figure 7E2). The differences in light propagation between the inverted and conventional pattern were again insensitive to variations of the parameters mentioned above, as well as to slit width and additional or fewer numbers of tiers used (Figure S12). Importantly, reduction of scatter in columns of inverted nuclei was robust against the irregularity of columns. In native nocturnal retina, columns of rod nuclei are fairly regular, as one can see, e.g., at the borders of clones of retinal cells labeled by a transgenic marker (Reese et al. [1995], Figures 1a and 1b; Acosta et al. [2008], Figures 2 and 3). Even when the centers of the nuclei in simulations were randomly displaced to a degree actually exceeding that observed in mouse retina, scatter remained low in lattices of inverted nuclei, despite notable deformation of the light path (Figures 7E3 and S12B).

Finally, inverted rod nuclei with ellipsoidal shape and a "bipartite" mass of constitutive heterochromatin (e.g., rabbit; c.f. Figure S6A) always have the main symmetry axis oriented along the physiological direction of light propagation (Figure 7D2). In 4-week-old mice, when nearly half of the rods still have two chromocenters, nuclei have the same ordered orientation (Figure 7D3), so that chromocenters still form columns. Notably, full visual ability is not reached in mouse before the age of 3.5–4 weeks (Prusky et al., 2004), i.e., the time when this regular arrangement of chromocenters is achieved.

DISCUSSION

Our study revealed a compelling correlation between the inverted nuclear architecture in mammalian rods and nocturnal vision. To test the optical interpretation of the inverted pattern, we investigated and ruled out a number of alternative explanations. First, the small nuclear size characteristic of rods with the inverted pattern per se does not cause the inverted architecture. Lymphocyte nuclei from spleen (probably the smallest nuclei in mouse) have a conventional pattern with a wide peripheral heterochromatin layer (Figure S13). The conventional pattern also occurs in other small mouse nuclei, e.g., granular cells in cerebellum (data not shown). In orthochromatophilic erythroblasts (i.e., before extrusion of the nucleus), the size of the nuclei reduces dramatically and large masses of heterochromatin accumulate in their internal regions; however, these masses of heterochromatin retain a connection to the heterochromatin lining most of the nuclear periphery, which is clearly different from the inverted pattern (Figure S13). Second, one could relate the inverted pattern to the association of highly transcribed genes with nuclear pores (Akhtar and Gasser, 2007; Sexton et al., 2007). Indeed, both rod and cone photoreceptors show a very high overall transcription level (Corbo and Cepko, 2005) because the membrane disks of the outer segments (sensory machinery proper) are continuously renewed, so that photoreceptor cells function as a kind of intensely working apocrine glands. Cone nuclei, however, always show a conventional pattern (Figure S2), as do all apocrine glands and the rods of diurnal mammals. In summary, only the correlation of the inverted pattern with nocturnal vision withstood testing.

The Effect of the Inverted Nuclear Architecture on the Optical Properties of the Retina

In the vertebrate eye, light must pass through the entire retina to reach the light-sensitive outer segments of photoreceptor cells (Figure 1). This design reflects the eye's evolutionary history and was optimized by elaborate adaptations at both neurobiological and optical levels (Sterling, 2003). A telling example is the diurnal tree shrew. The inner segments of its cones contain highly refractive giant mitochondria. They are remarkably similar to the inverted rod nuclei (Knabe et al. [1997], Figure 2b) and arguably function as lenses channeling light to the outer segments.

The small size characteristic of nuclei with the inverted pattern (Figures 4G and 5F) results in a higher average mass density of the central mass of highly refractive heterochromatin, augmenting the proposed optical effect (its refractive index is likely specifically increased because of the accumulation of proteins, data not shown). Furthermore, the small size of rod perikarya reduces thickening of the ONL because of increased areal density of rods. Our computer simulations suggest that the main consequence of the inverted pattern in rod nuclei is reduced scattering of light in the ONL. There are several putative mechanisms to translate reduced scattering in the ONL into an advantage for vision at low-light conditions (e.g., reduced photon loss), but the discussion of this issue is outside the scope of the present work. The biological importance of reduced scatter may be highlighted by comparison with the fovea, the small region of primate retina responsible for high-acuity vision. In the fovea, the problem of light scatter by retinal layers underlying the photoreceptor cells is solved radically: these layers are shifted laterally from the fovea. It is noteworthy that an optimized propagation of light through the ONL, together with a similar

code shows quantitative phase shift in radians. C3 shows phase profiles along the lines indicated in C2. C4 shows finite-difference time-domain (FDTD) simulation of light passage through objects with the phase retardation profiles shown in C3. Black horizontal lines show the width of the retardation area corresponding to the retardation profiles for the respective nuclei. The color scale shows the light intensity (normalized to the incident intensity).

(D) Columns formed by rod nuclei in the retina of adult (9 month) mouse (D1), adult rabbit (D2), and young adult (P28) mouse (D3). Note that the long axes of rod nuclei with bipartite heterochromatin masses (rabbit, c.f. Figures 5C and S6) and with two chromocenters (young mouse, c.f. Figure 4) are always oriented along the direction of light propagation. Scale bars represent 10 μm in D1 and D2 and 5 μm in D3.

(E) FDTD simulations of light propagation from a narrow source through ONL of nuclei with the conventional pattern (E1) and inverted pattern with moderate (E2) or strong (E3) deviations of nuclear centers from the regular lattice. Intensity profiles and color code are as in (B).

ability discussed earlier for other retinal layers (see Sterling, 2003; Franze et al., 2007), would provide an effective optical path through the entire nocturnal retina (Figure S14). Although both optical organization of the retina and processing of signals from individual rod cells still have to be understood, taken together, the above facts well support the conclusion that the nuclear architecture of rods was indeed adapted to improve the properties of the retina as an optical system.

Inverted and Conventional Nuclear Architecture: A Comparison

Amazingly, the inverted rod nuclei remain fully functional despite a dramatic change of the nuclear architecture. However, a certain position is not indispensable for transcription. Genes normally transcribed in the nuclear interior may remain active after experimental anchoring to the nuclear periphery (Finlan et al., 2008; Kumaran and Spector, 2008), while disruption of the tethering to the nuclear periphery may be insufficient for transcriptional activation (Gartenberg et al., 2004). An internal position of a gene appears to be more important for a high transcription level than for transcriptional activation (Ragoczy et al., 2006). Rod nuclei with the inverted architecture might predominantly switch to some alternative mechanisms of transcriptional regulation. Our results showed doubtlessly that in mouse rods all active and silent genes were localized in a peripheral shell (Figures 2A–2C and 2G). So far, we have found no indication that the transcriptional status of a gene in the inverted nucleus is related to its position within this shell (Figure 2G).

In mammalian mitotic chromosomes, gene-poor and gene-rich regions alternate as G and R bands (Figure 4I). Spatial separation of heterochromatic and euchromatic domains in the interphase and G0, associated with distinct differences in the replication timing (Ferreira et al., 1997; Sadoni et al., 1999) and in the distribution within the chromosome territories (Kupper et al., 2007), is a universal characteristic of eukaryotic nuclei with the conventional architecture (see Introduction). In explanation of this separation, it has been suggested that chromosomes meander in interphase nucleus from one domain to the other in a zigzag fashion (Figure 4J) (Chadwick and Willard, 2004). Our data on rod nuclei are fully consistent with such a scheme (Figure 4K): it is the nuclear positions and orientation of chromosome territories that are different between the two patterns.

The inverted nuclear architecture is unique to mammalian rod cells. Our results clearly show that despite the strong evolutionary conservation of the conventional pattern, nuclear architecture in rod cells was modified several times in the evolution of mammals (Figure 6A). Taken together, paleontological, molecular, and morphological data (Figure S15 and the accompanying discussion) strongly suggest (1) that the inverted pattern appeared very early in the evolution of mammals as an adaptation to nocturnal vision in this primarily nocturnal group of animals, (2) that, correspondingly, the conventional pattern was repeatedly reacquired (together with other characteristic features of the diurnal retina) in mammals that readopted a diurnal lifestyle (c.f. Figure 6), and (3) that restoration of the conventional architecture most likely demanded selective pressure for the conventional nuclear architecture (rather than simple accumulation of deleterious mutations). Comparison of the inverted and conventional patterns can therefore highlight the advantageous features that predetermine the nearly universal prevalence of the conventional nuclear architecture.

One of the parameters of nuclear architecture that is re-established in diurnal mammals is simply a more typical nuclear size (Figure 5F). Functional significance of the nuclear size has so far attracted very little attention. Another recovered feature is the conventional pattern itself. Specific nuclear positions ensuring spatial separation of transcriptionally active and inactive chromatin (Kosak et al., 2007; Lanctot et al., 2007), as well as direct spatial nuclear interactions between genes (Fraser and Bickmore, 2007; Sexton et al., 2007), was recently recognized as an important factor in transcriptional regulation. Nuclear architecture determines the landscape for these spatial interactions (Cremer and Cremer, 2001; Cremer et al., 2006). The inverted pattern causes a uniform petal-like chromosome arrangement that strongly reduces the diversity of chromosome neighborhoods compared to the conventional pattern (Figures 4J and 4K). Therefore, the reason for the nearly absolute prevalence of the conventional architecture in eukaryotic nuclei might be increased opportunities for ''gene regulation through nuclear organization'' (Sexton et al., 2007) suggested by the conventional pattern.

EXPERIMENTAL PROCEDURES

Animals and Histology

Mice (inbred strain C57Bl6 or outbred strain ICR/CD1) were killed by cervical dislocation. Retina was excised and fixed in 4% formaldehyde in PBS for one day. Vibratome sections (20–30 μm) and cryosections (20 μm) were prepared by standard protocols. Cryosections were stored at −80°C. Other species (see Table S2) were studied on cryosections. Areal densities of photoreceptors were estimated with whole mounts of retina.

Immunostaining and FISH

Before immunostaining, sections were air dried for 30 min, and antigen retrieval was performed by heating in 10 mM sodium citrate buffer at 80°C for 5 min, unless specified otherwise. For more details and the antibodies used, see the Supplemental Experimental Procedures. The used protocols for DNA FISH are available online (Cremer et al., 2007; Solovei et al., 2007). The protocol for RNA FISH was adopted from that of R. Singer laboratory (http://singerlab.aecom.yu.edu/protocols/). In brief, whole mouse eyes were dissected, fixed in 3.7% formaldehyde/10% acetic acid/1× PBS for 15 min at room temperature, washed twice with PBS, immediately embedded in Jung Tissue Freezing Medium (Leica Microsystems), and frozen.

Microscopy and Image Analysis

Image stacks were collected with a Leica TCS SP2 confocal microscope with Plan Apo 63×/1.4 NA oil immersion objective. After correction for chromatic shift and segmentation of the nuclear border with Amira 4 TGS software, radial distribution of FISH signals was quantified with in-house relative radial distribution (RRD) and absolute distance to surface (ADS) programs.

Quantitative Phase Measurements and Computer Simulations

Rod cells were isolated from fresh mouse and pig retina and immediately imaged in PBS with a compensated Jamin-Lebedev interferometric microscope (Zeiss). The raw images were quantitatively analyzed as described in the Supplemental Data. Optical computer simulations were performed with a 2D FDTD algorithm (“Meep FDTD package,” http://jdj.mit.edu/meep/; see also Farjadpour et al. [2006]).

For details on all methods used, see the Supplemental Experimental Procedures.

SUPPLEMENTAL DATA

Supplemental Data include Supplemental Experimental Procedures, 15 figures, and two tables and can be found with this article online at http://www.cell.com/supplemental/S0092-8674(09)00137-8.

ACKNOWLEDGMENTS

We thank A.H.F.M. Peters (FMI for Biomedical Research, Basel) for antibodies against H3K9me3 and H4K20me3, M. Hess (University of Munich) for initial help with mouse retina, S. Heynck (MPI for Brain Research, Frankfurt) for perfect sectioning, all colleagues who kindly supplied us mammal retina material (see Table S2), S. Haverkamp (MPI for Brain Research) for a TEM image of mouse rod perykarion, B. Amos (MRC LMB, Cambridge, UK) for help with the Jamin-Lebedev microscope, and M. Gerard (Abattoir Haverhill) for the provision of pig eyes. We are grateful to D. Sheer (Queen Mary's School of Medicine and Dentistry, London), A. Reichenbach (University of Leipzig), W. Stephan (University of Munich), and T.D. Lamb (Australian National University, Canberra) for reading of the manuscript and/or critical comments. The study was supported by Deutsche Forschungsgemeinschaft grant Cr59/20 and Bundesministerium für Bildung und Forschung NGFN II-EP grant 0213377A to T.C., fellowships from the Instituts de recherche en santé du Canada and the Humboldt Stiftung to C.L., and Engineering and Physical Sciences Research Council and Cambridge European Trust scholarships to M.K.

Received: July 20, 2007
Revised: December 17, 2008
Accepted: January 27, 2009
Published: April 16, 2009

REFERENCES

Acosta, M.L., O'Brien, K.M.B., Tan, S.-S., and Kalloniatis, M. (2008). Emergence of cellular markers and functional ionotropic lutamate receptors on tangentially dispersed cells in the developing mouse retina. J. Comp. Neurol. *506*, 506–523.

Ahnelt, P.K., and Kolb, H. (2000). The mammalian photoreceptor mosaic-adaptive design. Prog. Retin. Eye Res. *19*, 711–777.

Akhtar, A., and Gasser, S.M. (2007). The nuclear envelope and transcriptional control. Nat. Rev. Genet. *8*, 507–517.

Blackshaw, S., Fraioli, R.E., Furukawa, T., and Cepko, C.L. (2001). Comprehensive analysis of photoreceptor gene expression and the identification of candidate retinal disease genes. Cell *107*, 579–589.

Carter-Dawson, L.D., and LaVail, M.M. (1979). Rods and cones in the mouse retina. I. Structural analysis using light and electron microscopy. J. Comp. Neurol. *188*, 245–262.

Chadwick, B.P., and Willard, H.F. (2004). Multiple spatially distinct types of facultative heterochromatin on the human inactive X chromosome. Proc. Natl. Acad. Sci. USA *101*, 17450–17455.

Chuang, C.H., Carpenter, A.E., Fuchsova, B., Johnson, T., de Lanerolle, P., and Belmont, A.S. (2006). Long-range directional movement of an interphase chromosome site. Curr. Biol. *16*, 825–831.

Corbo, J.C., and Cepko, C.L. (2005). A hybrid photoreceptor expressing both rod and cone genes in a mouse model of enhanced S-cone syndrome. PLoS Genet. *1*, e11.

Cremer, T., and Cremer, C. (2001). Chromosome territories, nuclear architecture and gene regulation in mammalian cells. Nat. Rev. Genet. *2*, 292–301.

Cremer, T., Cremer, M., Dietzel, S., Muller, S., Solovei, I., and Fakan, S. (2006). Chromosome territories–a functional nuclear landscape. Curr. Opin. Cell Biol. *18*, 307–316.

Cremer, M., Müller, S., Köhler, D., Brero, A. and Solovei, I. (2007). Cell Preparation and Multicolor FISH in 3D Preserved Cultured Mammalian Cells. Cold Spring Harbor Protocols. 10.1101/pdb.prot4723.

Dundr, M., Ospina, J.K., Sung, M.H., John, S., Upender, M., Ried, T., Hager, G.L., and Matera, A.G. (2007). Actin-dependent intranuclear repositioning of an active gene locus in vivo. J. Cell Biol. *179*, 1095–1103.

Farjadpour, A., Roundy, D., Rodriguez, A., Ibanescu, M., Bermel, P., Joannopoulos, J.D., Johnson, S.G., and Burr, G.W. (2006). Improving accuracy by subpixel smoothing in the finite-difference time domain. Opt. Lett. *31*, 2972–2974.

Ferreira, J., Paolella, G., Ramos, C., and Lamond, A.I. (1997). Spatial organization of large-scale chromatin domains in the nucleus: a magnified view of single chromosome territories. J. Cell Biol. *139*, 1597–1610.

Finlan, L.E., Sproul, D., Thomson, I., Boyle, S., Kerr, E., Perry, P., Ylstra, B., Chubb, J.R., and Bickmore, W.A. (2008). Recruitment to the nuclear periphery can alter expression of genes in human cells. PLoS Genet. *4*, e1000039.

Franze, K., Grosche, J., Skatchkov, S.N., Schinkinger, S., Foja, C., Schild, D., Uckermann, O., Travis, K., Reichenbach, A., and Guck, J. (2007). Muller cells are living optical fibers in the vertebrate retina. Proc. Natl. Acad. Sci. USA *104*, 8287–8292.

Fraser, P., and Bickmore, W. (2007). Nuclear organization of the genome and the potential for gene regulation. Nature *447*, 413–417.

Gartenberg, M.R., Neumann, F.R., Laroche, T., Blaszczyk, M., and Gasser, S.M. (2004). Sir-mediated repression can occur independently of chromosomal and subnuclear contexts. Cell *119*, 955–967.

Gregory, T.R., Nicol, J.A., Tamm, H., Kullman, B., Kullman, K., Leitch, I.J., Murray, B.G., Kapraun, D.F., Greilhuber, J., and Bennett, M.D. (2007). Eukaryotic genome size databases. Nucleic Acids Res. *35*, D332–D338.

Guelen, L., Pagie, L., Brasset, E., Meuleman, W., Faza, M.B., Talhout, W., Eussen, B.H., de Klein, A., Wessels, L., de Laat, W., and van Steensel, B. (2008). Domain organization of human chromosomes revealed by mapping of nuclear lamina interactions. Nature *453*, 948–951.

Helmlinger, D., Hardy, S., Abou-Sleymane, G., Eberlin, A., Bowman, A.B., Gansmuller, A., Picaud, S., Zoghbi, H.Y., Trottier, Y., Tora, L., and Devys, D. (2006). Glutamine-expanded ataxin-7 alters TFTC/STAGA recruitment and chromatin structure leading to photoreceptor dysfunction. PLoS Biol. *4*, e67.

Knabe, W., Skatchkov, S., and Kuhn, H.J. (1997). "Lens mitochondria" in the retinal cones of the tree-shrew Tupaia belangeri. Vision Res. *37*, 267–271.

Kosak, S.T., Scalzo, D., Alworth, S.V., Li, F., Palmer, S., Enver, T., Lee, J.S., and Groudine, M. (2007). Coordinate gene regulation during hematopoiesis is related to genomic organization. PLoS Biol. *5*, e309.

Kumaran, R.I., and Spector, D.L. (2008). A genetic locus targeted to the nuclear periphery in living cells maintains its transcriptional competence. J. Cell Biol. *180*, 51–65.

Kupper, K., Kolbl, A., Biener, D., Dittrich, S., von Hase, J., Thormeyer, T., Fiegler, H., Carter, N.P., Speicher, M.R., Cremer, T., and Cremer, M. (2007). Radial chromatin positioning is shaped by local gene density, not by gene expression. Chromosoma *116*, 285–306.

Lanctot, C., Cheutin, T., Cremer, M., Cavalli, G., and Cremer, T. (2007). Dynamic genome architecture in the nuclear space: regulation of gene expression in three dimensions. Nat. Rev. Genet. *8*, 104–115.

Martens, J.H., O'Sullivan, R.J., Braunschweig, U., Opravil, S., Radolf, M., Steinlein, P., and Jenuwein, T. (2005). The profile of repeat-associated histone lysine methylation states in the mouse epigenome. EMBO J. *24*, 800–812.

Misteli, T. (2007). Beyond the sequence: cellular organization of genome function. Cell *128*, 787–800.

Murphy, W.J., Eizirik, E., O'Brien, S.J., Madsen, O., Scally, M., Douady, C.J., Teeling, E., Ryder, O.A., Stanhope, M.J., de Jong, W.W., and Springer, M.S. (2001). Resolution of the early placental mammal radiation using Bayesian phylogenetics. Science *294*, 2348–2351.

Peichl, L. (2005). Diversity of mammalian photoreceptor properties: adaptations to habitat and lifestyle? Anat. Rec. A Discov. Mol. Cell. Evol. Biol. *287*, 1001–1012.

Postberg, J., Alexandrova, O., Cremer, T., and Lipps, H.J. (2005). Exploiting nuclear duality of ciliates to analyse topological requirements for DNA replication and transcription. J. Cell Sci. *118*, 3973–3983.

Prusky, G.T., Alam, N.M., Beekman, S., and Douglas, R.M. (2004). Rapid quantification of adult and developing mouse spatial vision using a virtual optomotor system. Invest. Ophthalmol. Vis. Sci. *45*, 4611–4616.

Ragoczy, T., Bender, M.A., Telling, A., Byron, R., and Groudine, M. (2006). The locus control region is required for association of the murine beta-globin locus with engaged transcription factories during erythroid maturation. Genes Dev. *20*, 1447–1457.

Reddy, K.L., Zullo, J.M., Bertolino, E., and Singh, H. (2008). Transcriptional repression mediated by repositioning of genes to the nuclear lamina. Nature *452*, 243–247.

Reese, B.E., Harvey, A.R., and Tan, S.S. (1995). Radial and tangential dispersion patterns in the mouse retina are cell-class specific. Proc. Natl. Acad. Sci. USA *92*, 2494–2498.

Ronneberger, O., Baddeley, D., Scheipl, F., Verveer, P.J., Burkhardt, H., Cremer, C., Fahrmeir, L., Cremer, T., and Joffe, B. (2008). Spatial quantitative analysis of fluorescently labeled nuclear structures: Problems, methods, pitfalls. Chromosome Res. *16*, 523–563.

Sadoni, N., Langer, S., Fauth, C., Bernardi, G., Cremer, T., Turner, B.M., and Zink, D. (1999). Nuclear organization of mammalian genomes. Polar chromosome territories build up functionally distinct higher order compartments. J. Cell Biol. *146*, 1211–1226.

Sexton, T., Schober, H., Fraser, P., and Gasser, S.M. (2007). Gene regulation through nuclear organization. Nat. Struct. Mol. Biol. *14*, 1049–1055.

Solovei, I., Grasser, F., and Lanctôt, C. (2007). FISH on Histological Sections. Cold Spring Harbor Protocols. 10.1101/pdb.prot4729.

Sterling, P. (2003). How retinal circuits optimize the transfer of visual information. In The Visual Neurosciences, L.M. Chalupa and J.S. Werner, eds. (Cambridge, MA: MIT Press), pp. 234–259.

Takizawa, T., Gudla, P.R., Guo, L., Lockett, S., and Misteli, T. (2008). Allele-specific nuclear positioning of the monoallelically expressed astrocyte marker GFAP. Genes Dev. *22*, 489–498.

Waterston, R.H., Lindblad-Toh, K., Birney, E., Rogers, J., Abril, J.F., Agarwal, P., Agarwala, R., Ainscough, R., Alexandersson, M., An, P., et al. (2002). Initial sequencing and comparative analysis of the mouse genome. Nature *420*, 520–562.

Williams, R.W., and Moody, S.A. (2003). Developmental and genetic control of cell number in the retina. In The Visual Neurosciences, L.M. Chalupa and J.S. Werner, eds. (Cambridge, MA: MIT Press), pp. 65–78.

Zhang, L.F., Huynh, K.D., and Lee, J.T. (2007). Perinucleolar targeting of the inactive X during S phase: evidence for a role in the maintenance of silencing. Cell *129*, 693–706.